hand, the catalyzed oxidation currents were reproduceable at the PB-modified electrodes.

Eventually, we conclude that the oxidized form of PB is one of the best catalysts toward H_2O_2 oxidation in acidic solutions. It is reasonable to believe that the catalyzed oxidation of H_2O_2 proceeds in crystals of the oxidized form of PB just as expected for the reduction of H_2O_2, because the catalyzed oxidation also showed first-order dependence on the concentrations of H_2O_2 and Γ_{PB}.

It is noteworthy that the stability of the catalyst represented here was excellent under certain conditions. The stability of the wave of PB itself was extremely high as described in our previous papers.[8] For this reason, the PB-modified electrode can be applied in an electrochromic display device.[8a] Toward O_2 reduction, a lifetime experiment showed that only a few percent decrease in the catalyzed current was observed after 30 h holding the electrode potential at −0.2 V vs. SCE. Such a high durability should be important for its application such as fuel cells and air batteries. However, we found a gradual loss in activity when a large amount of PB (20 mC/cm^2) was employed in order to obtain higher current densities. When observed under a microscope, the film of PB was sometimes partially removed. This behavior may be explained by poor adhesion of the PB film on the GC surface.

Finally, we briefly mention Prussian blue analogues. It has already been shown that iron–ruthenium cyanide (ruthenium purple; RP), $Fe_4^{3+}[Ru^{II}(CN)_6]_3$, and iron–osmium cyanide, $Fe_4^{3+}[Os^{II}(CN)_6]_3$, can be prepared by an electrochemical method.[19] It was found that both were active for the reduction of O_2. Applications as catalysts can be readily expected from the above results.

Acknowledgment. We acknowledge Professors R. M. De La Rue (Glasgow) and T. Osa (Tohoku) for comments on this manuscript.

Registry No. Fe, 7439-89-6; O_2, 7782-44-7; H_2O_2, 7722-84-1; H_2O, 7732-18-5; C, 7440-44-0; PB, 12240-15-2; Prussian white, 81681-39-2.

Structure of C_{3v} P horanyl and C_{4v} Phosphorane Anion Radicals. A Quai Chemical Study

R. A. J. Janssen,* G. J. Visser, and H. M. Buck

Contribution from the Department of Organic Chemistry, Eindhoven University of Technology, Eindhoven, The Netherlands 5600 MB. *Received September 28, 1983*

Abstract: Ab initio molecular orbital calculations on various C_{3v} phosphoranyl radicals and the C_{4v} $\dot{P}F_5^-$ phosphorane anion radical are presented. By the unrestricted Hartree–Fock method with a 4-31G basis set the geometries for C_{3v} $X^a\dot{P}X^e_3$ (X^a = apical ligand, X^e = equatorial ligand) radicals were optimized for X = H, F, and Cl. All C_{3v} radicals reveal a trigonal-bipyrimidal structure with the unpaired electron in apical position. The optimized $\dot{P}F_5^-$ radical is octahedral with the unpaired electron acting as a ligand. The calculated isotropic hyperfine coupling constants are in good agreement with the experimental values. Variation of the apical–equatorial bond angle for $H\dot{P}H_3$ and $\dot{P}F_5^-$ leads to σ^*-arrangements. A detailed study of the C_{3v} $PH_3 + H\cdot$ potential energy surface is described. It appears that a σ^*-arrangement is not stable but leads to dissociation. The stability of $X^a\dot{P}H_3$ with respect to dissociation into PH_3 and $X^a\cdot$ is described, and transition states are calculated. $H\dot{P}H_3$ lies 43.2 kJ mol^{-1} below its transition state, $F\dot{P}H_3$ (9.8 kJ mol^{-1}), whereas $Cl\dot{P}H_3$ is unstable.

I. Introduction

A number of single-crystal ESR studies have shown that phosphoranyl radicals ($\dot{P}X_4$) can adopt different configurations depending on the ligands attached to phosphorus and steric constraints of ring structures.[1-4] Most frequently a C_{2v} geometry is encountered. The electronic structure of these C_{2v} phosphoranyl radicals is well established and may be described as a trigonal bipyramid (TBP) with the unpaired electron acting as a fifth ligand in an equatorial position.[2,5-7] In contrast to the structure of C_{2v} phosphoranyl radicals, conflicting ideas exist on the electronic structure of phosphoranyl radicals with a C_{3v} geometry and phosphorane anion radicals with a C_{4v} geometry. The unpaired electron in the $Ph_3\dot{P}Cl$ radical, which possesses a C_{3v} geometry, is believed to reside in a σ^* P–Cl orbital,[3] accounting for the high spin density found on chlorine and the fact that the ^{31}P tensor

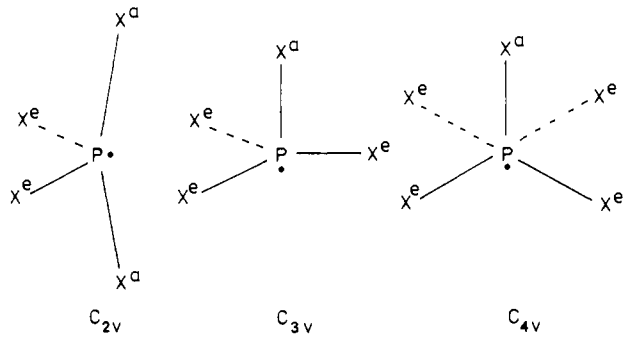

is parallel to the ^{35}Cl tensor. By contrast the extensive studies on the C_{3v} radical $\cdot\overline{P(OCH_2CH_2)_3N^+}BF_4^-$ show unambiguously

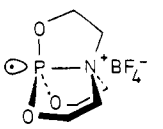

that the unpaired electron resides in the apical position of a TBP (TBP-a).[1,8] The near isotropic ^{14}N hyperfine coupling of 22 G

(1) Hamerlinck, J. H. H.; Schipper, P.; Buck, H. M. *J. Am. Chem. Soc.* **1983**, *105*, 385.
(2) Hasegawa, A.; Ohnishi, K.; Sogabe, K.; Miura, M. *Mol. Phys.* **1975**, *30*, 1367.
(3) Berclaz, T.; Geoffroy, M.; Lucken, E. A. C. *Chem. Phys. Lett.* **1975**, *36*, 677.
(4) Gillbro, T.; Williams, F. *J. Am. Chem. Soc.* **1974**, *96*, 5032.
(5) Colussi, A. J.; Morton, J. R.; Preston, K. F. *J. Phys. Chem.* **1975**, *79*, 1855.
(6) Hamerlinck, J. H. H.; Hermkens, P. H. H.; Schipper, P.; Buck, H. M. *J. Chem. Soc., Chem. Commun.* **1981**, 358.
(7) Howell, J. M.; Olsen, J. F. *J. Am. Chem. Soc.* **1976**, *98*, 7119.
(8) Hamerlinck, J. H. H.; Schipper, P.; Buck, H. M. *J. Am. Chem. Soc.* **1980**, *102*, 5679.

0002-7863/84/1506-3429$01.50/0

Table I. Optimized Geometries, UHF Energies, and $\langle S^2 \rangle$ Values of the C_{3v} $X^aPX^e_3$ Radicals[a]

$X^aPX^e_3$	P–X^a	P–X^e	ϕ	E(UHF)	$\langle S^2 \rangle$
HPH_3	1.43	1.59	89.5	−342.472475	0.8328
FPH_3	1.79	1.43	85.7	−441.245124	0.7579
$ClPH_3$					
HPF_3	1.39	1.70	92.7	−638.782736	0.7787
FPF_3	1.61	1.67	91.6	−737.549048	0.7798
$ClPF_3$	2.21	1.69	92.0	−1097.199849	0.7981
$HPCl_3$	1.42	2.35	93.9	−1717.851382	0.9580
$FPCl_3$	1.64	2.36	95.7	−1816.599229	1.0054
$ClPCl_3$	2.22	2.39	98.7	−2176.272556	1.0907

[a] Bond lengths in angstroms, bond angles in degrees, and UHF energies in atomic units.

Table II. Fermi Contact Integrals $\rho(\vec{R}_{Nucl})$[a] and Isotropic Hyperfine Coupling Constants a_{Nucl}^{iso}[b] of the C_{3v} $X^aPX^e_3$ Radicals

	P		X^a		X^e	
	$\rho(\vec{R}_P)$	a_P^{iso}	$\rho(\vec{R}_{X^a})$	$a_{X^a}^{iso}$	$\rho(\vec{R}_{X^e})$	$a_{X^e}^{iso}$
HPH_3	1.252	809	0.007	12	0.125	199
FPH_3	0.280	181	0.195	292	0.048	77
HPF_3	2.032	1313	−0.013	−22	0.158	237
FPF_3	1.920	1241	−0.019	−29	0.152	228
$ClPF_3$	2.006	1296	0.007	1	0.154	232
$HPCl_3$	1.400	905	−0.005	−8	0.048	8
$FPCl_3$	1.218	787	−0.055	−82	0.042	7
$ClPCl_3$	1.357	903	−0.027	−41	0.042	7

[a] $\rho(\vec{R}_{Nucl})$ in electrons Bohr^{-3}. [b] a_{Nucl}^{iso} in gauss.

indicates a small spin density on the apical nitrogen atom. Similar differences in the structure of C_{4v} phosphorane anion radicals (PX_5^-) have been reported. The isotropic hyperfine pattern of the PF_5^- radical anion shows four equivalent equatorial fluorines with a large coupling and one with a small coupling arising from the unique apical fluorine.[9] The same structure has been proposed for PCl_5^-[10] and the isoelectronic SF_5.[11] For the $ClP(O_2C_6H_4)_2^-$ radical, which adopts a local C_{4v} symmetry with chlorine in the

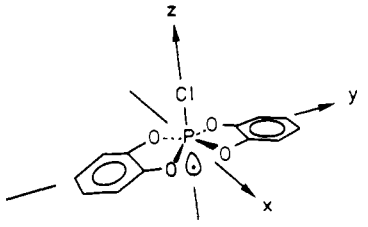

apical position, the ^{31}P, ^{35}Cl, and ^{37}Cl tensors are coincident and directed along the P–Cl linkage.[12] The chlorine hyperfine coupling shows in sharp contrast to PF_5^- a large spin density on the apical ligand. The aim of this ab initio study is to shed some light on these confusing differences and to examine the preferred geometries and electronic structures of various C_{3v} an C_{4v} radicals. A detailed study is made of the C_{3v} PH_3 + H· potential energy surface. The stability of C_{3v} radicals HPH_3, FPH_3, and $ClPH_3$ is discussed.

II. Quantum Chemical Methods

The calculations were performed with the GAUSSIAN76[13] and GAUSSIAN80[14] program systems using the unrestricted Hartree–Fock (UHF) procedure. Throughout a split valence 4-31G basis set was used. The structures were fully optimized with respect to all bond lengths and bond angles within the symmetry constraints. Isotropic hyperfine coupling constants (a_{Nucl}^{iso}) were calculated from the Fermi contact integrals ($\rho(\vec{R}_{Nucl})$):

$$\rho(\vec{R}_{Nucl}) = \sum_{\mu,\nu} P_{\mu\nu}^{\alpha-\beta} \phi_\mu(\vec{R}_{Nucl}) \phi_\nu(\vec{R}_{Nucl}) \quad (1)$$

$$a_{Nucl}^{iso} = (4\pi/3) g\beta\gamma_{Nucl} \langle S_z \rangle^{-1} \rho(\vec{R}_{Nucl}) \quad (2)$$

in which $P_{\mu\nu}^{\alpha-\beta}$ is the first-order spin density matrix and ϕ_μ and ϕ_ν are the atomic basis functions. Orbital spin densities were obtained by performing a Mulliken population analysis on the single determinant wave function. Correlation energies were calculated by Møller–Plesset perturbation theory to second and third order (UMP2 and UMP3) and by configuration interaction with all double substitutions (CID). Transition states were calculated with the GAUSSIAN80 saddle-point-search algorithm. At stationary points the second derivative matrix possesses a single negative value.

III. Geometry and Electronic Structure

(1) Optimized Geometries for C_{3v} Radicals. The geometries of the radicals $X^aPX^e_3$ have been optimized for all combinations

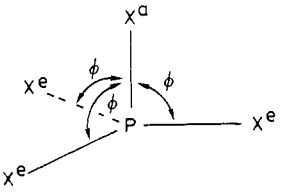

of X^a and X^e with X = H, F, or Cl within a C_{3v} symmetry constraint.[15] The optimized parameters for these radicals are collected in Table I together with the calculated UHF energies and the expectation values of S^2. The geometric parameters for HPH_3 and FPF_3 differ slightly from those previously reported by Howell et al.,[7] because in our study we included the apical–equatorial bond angle (ϕ) in the optimization. For $ClPH_3$ no stable geometry could be calculated (vide infra). Characteristic for all these C_{3v} radicals is the apical–equatorial bond angle ϕ that is near to 90°.

The singly occupied molecular orbital (SOMO) determines the distribution of the unpaired electron in the radical. *The calculated*

(9) Morton, J. R.; Preston, K. F.; Strach, S. J. *J. Magn. Reson.* **1980**, *37*, 321.
(10) Mishra, S. P.; Symons, M. C. R. *J. Chem. Soc., Dalton Trans.* **1976**, 139.
(11) Hasegawa, A.; Williams, F. *Chem. Phys. Lett.* **1977**, *45*, 275.
(12) Hamerlinck, J. H. H.; Schipper, P.; Buck, H. M. *Chem. Phys. Lett.* **1981**, *80*, 358.
(13) Binkely, J. S.; Whiteside, R. A.; Hariharan, P. C.; Seeger, R.; Pople, J. A.; Hehre, W. J.; Newton, M. D. *QCPE* **1978**, *11*, 368.
(14) Binkely, J. S.; Whiteside, R. A.; Krishnan, R.; Seeger, R.; DeFrees, D. J.; Schlegel, H. B.; Topiol, S.; Kahn, L. R.; Pople, J. A. GAUSSIAN80, Department of Chemistry, Carnegie-Mellon University, Pittsburgh, 1980.

(15) Without this symmetry constraint optimization would probably reveal C_{2v} or C_s geometries (see, e.g., ref 2, 5, 7, and 10).

Table III. Valence Orbital Spin Densities of the C_{3v} $X^a\dot{P}X^e_3$ Radicals[a]

	P		X^a		X^e	
	3s	$3p_z$	ns	np_z	ns	np_e[b]
$H\dot{P}H_3$	0.08	0.20	−0.01		0.42	
$F\dot{P}H_3$	0.04	0.57	−0.01	0.11	0.13	
$H\dot{P}F_3$	0.31	0.37	0.04		0.00	0.16
$F\dot{P}F_3$	0.31	0.33	0.00	−0.02	0.00	0.16
$Cl\dot{P}F_3$	0.33	0.52	0.00	−0.10	−0.01	0.18
$H\dot{P}Cl_3$	0.10	0.14	0.01		−0.01	0.46
$F\dot{P}Cl_3$	0.06	0.12	0.01	−0.01	−0.01	0.50
$Cl\dot{P}Cl_3$	0.09	0.03	0.00	0.04	−0.01	0.55

[a] The listed values are summations over the inner and outer orbitals of the split valence 4-31G basis set. [b] np_e is the equatorial contribution, calculated as $np_x + np_y$.

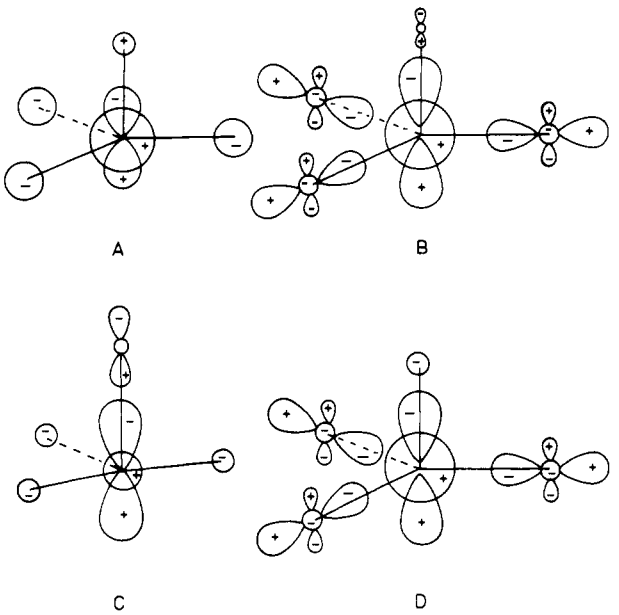

Figure 1. Schematic representation of the SOMOs of C_{3v} phosphoranyl radicals. (A) $H\dot{P}H_3$, (B) $F\dot{P}F_3$, (C) $F\dot{P}H_3$, (D) $H\dot{P}F_3$.

SOMOs indicate that all studied radicals have a TBP-a structure and not a σ-arrangement.* This is depicted in Figure 1, where a schematical representation of the SOMO is given for some of the studied radicals. To characterize the electronic structure of these C_{3v} phosphoranyl radicals, we calculated the Fermi contact integrals ($\rho(\vec{R}_{nucl})$) and the isotropic hyperfine coupling constants (a_{Nucl}^{iso}) together with the valence orbital spin densities. These values are given in Tables II and III. The listed values for the three $X^a\dot{P}Cl_3$ radicals must be regarded with some scepticism because the $\langle S^2 \rangle$ values of their wave functions include a considerable amount of contaminating higher multiplicities (Table I). It appears that roughly speaking all TBP-a radicals have a similar spin density distribution, in which the major part is located on phosphorus and the equatorial ligands. The apical ligand possesses a near zero spin density, which is a direct result of the fact that its atomic orbitals do not contribute significantly to the SOMO. This calculated general structure is in perfect agreement with the experimental values of the C_{3v} $\cdot\overline{P(OCH_2CH_2)_3N}^+BF_4^-$ radical and therefore confirms its assignment as TBP-a (vide supra).

In comparison with the other calculated C_{3v} radicals the electronic structure of $F\dot{P}H_3$ shows some remarkable differences. Relative to $H\dot{P}H_3$ there is a serious decrease of the contribution to the SOMO of the phosphorus 3s orbital and the 1s orbital of the equatorial hydrogen atoms. Simultaneously the contribution of the phosphorus $3p_z$ and of the apical ligand is increased. It has been frequently suggested by various authors[16-19] that a radical

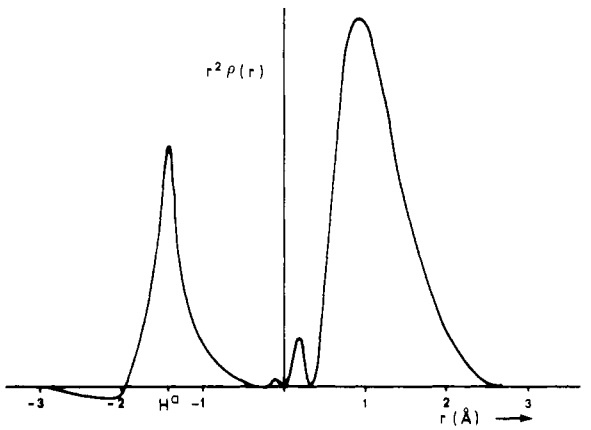

Figure 2. Radial spin density probability along the C_3 axis for the $H\dot{P}H_3$ radical.

like $F\dot{P}H_3$, with one strongly electronegative ligand, preferentially occupies a tetrahedral geometry with the unpaired electron in an antibonding σ* orbital. However, our calculations show that for $F\dot{P}H_3$ the optimized value of ϕ (85.9°) does not confirm a tetrahedral geometry and that the electronic structure of $F\dot{P}H_3$ is clearly TBP-a (Figure 1). In order to get an indication of the distance between phosphorus and the point of the maximum probability of finding the unpaired electron along the C_3 axis, we have calculated for $H\dot{P}H_3$ the radial spin density distribution $r^2\rho(r)$, where r is the radius centered on phosphorus and $\rho(r)$ is defined by eq 1 (section II). Figure 2 reveals that this distance is 0.93 Å. As can be seen from Table I the optimized apical bond length for those radicals where $X^a = X^e$ ($H\dot{P}H_3$, $F\dot{P}F_3$, and $Cl\dot{P}Cl_3$) is considerably shorter than the corresponding equatorial bond. In view of their TBP-a structures this is a remarkable result. It is a well-known fact that for pentacoordinated phosphorus compounds with a TBP geometry the axial bonds are longer than the equatorial bonds when identical ligands are involved.[20] The same bond-length rule applies for TBP-e (C_{2v}) phosphoranyl radicals as was shown by Howell et al.[7] The question arises of why the TBP-a radicals form an exception and possess a short apical bond. To answer this question one must be aware of the fact that both phosphoranyl radicals and pentacoordinated phosphorus compounds are hypervalent species with more than eight electrons around phosphorus. To accommodate the extra electron(s) the HOMO[21] will possess some antibonding character. For phosphoranyl radicals this HOMO is identical with the SOMO. The HOMOs for the PH_5 molecule and the C_{2v} and C_{3v} $\dot{P}H_4$ radicals are depicted in Figure 3. The schematic representations indicate that, for the three examples, in the ligands that contribute most to the HOMO the bond length is increased, while the ligands with a smaller contribution possess a normal bond length (ca. 1.43 Å).

(16) Symons, M. C. R. *Chem. Phys. Lett.* **1976**, *40*, 226.
(17) Penkovsky, V. V. *Dokl. Akad. Nauk. SSRR (Engl. Transl.)* **1978**, *243*, 539.
(18) Baban, J. A.; Roberts, B. P. *J. Chem. Soc., Chem. Commun.* **1979**, 537.
(19) Evans, J. C.; Mishra, S. P. *J. Inorg. Nucl. Chem.* **1981**, *43*, 481.
(20) Holmes, R. R. *ACS Monogr.* **1980**, *No.* 175.
(21) Abbreviations used are HOMO for highest occupied molecular orbital and LUMO for lowest unoccupied molecular orbital.

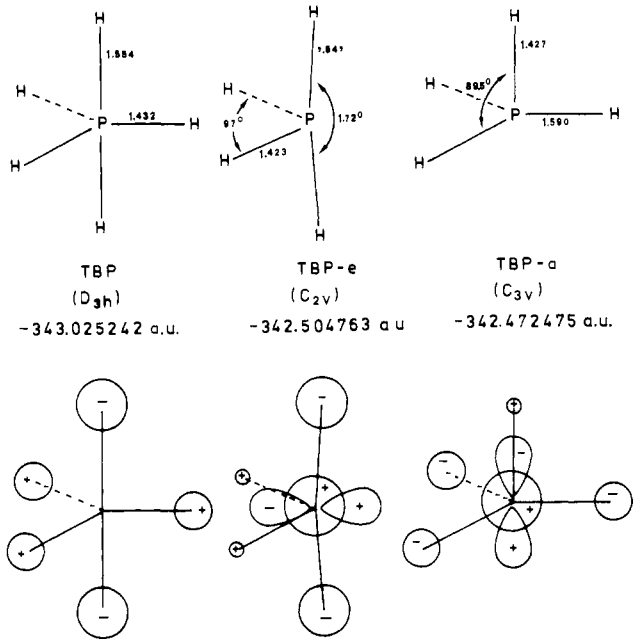

Figure 3. Geometries (ref 7, Table I) and calculated antibonding molecular orbitals of PH_5, C_{2v} $\dot{P}H_4$, and C_{3v} $\dot{P}H_4$.

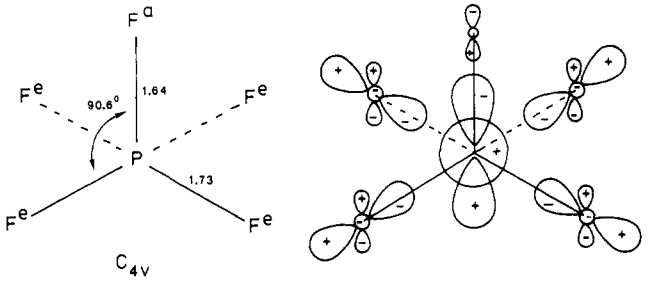

Figure 4. Optimized geometry of $\dot{P}F_5^-$ (E(UHF) = −836.982 786 au; $\langle S^2 \rangle$ = 0.7626) and a schematical representation of the SOMO.

It is obvious that the increased bond length is a direct result of the antibonding character. The participation of d orbitals in pentavalent phosphorus compounds is still a subject of controversy.[22-25] A number of ab initio studies on pentacoordinated phosphorus compounds[26-29] and phosphoranyl radicals[7] revealed that the principal concepts of the bonding are adequately described without the introduction of d functions. However, for numerically highly accurate results in the determination of bond lengths and bond energies they are found to be essential,[30] merely because their inclusion will increase the completeness of the basis set that is used. From Figure 3 it is clear that the symmetry of the HOMO of PH_5 fits exactly to the phosphorus $3d_{z^2}$ orbital, when this is

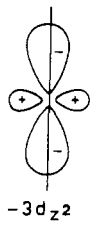

provided with a negative coefficient. Therefore the $3d_{z^2}$ orbital will contribute to some extent to the HOMO and thus to the bonding in PH_5.

(2) Optimized Structure for C_{4v} $\dot{P}F_5^-$. Optimization of $\dot{P}F_5^-$ within a C_{2v} symmetry constraint revealed an exact C_{4v} geometry. This optimized structure of $\dot{P}F_5^-$ is analogous to the C_{3v} optimized structure of $F\dot{P}F_3$. The bond angle between the apical bond and the four equatorial bonds is 90.6°, and again the apical bond is substantially shorter than the equatorial bond (Figure 4). This is in accordance with the fact that the equatorial ligands contribute more to the antibonding SOMO than the apical ligand. The calculated isotropic hyperfine coupling constants are in good agreement with the experimental values[9] (Table IV). The SOMO of the $\dot{P}F_5^-$ phosphorane anion radical indicates that this radical can be described as octahedral (O_h) with the unpaired electron acting as a sixth ligand. The electronic structure of $\dot{P}F_5^-$ is essentially the same as for the TBP-a radicals, in which phosphorus and the equatorial fluorines possess a large spin density and the apical ligand a very small spin density.

(3) Geometry Variations and Electronic Structures. Until now all calculations revealed radicals in which the unpaired electron occupies an orbital directed toward the missing ligand of a TBP or O_h structure. This resulted in a small spin density on the apical ligand. In a σ^* structure the unpaired electron occupies an an-

Table IV. Experimental[a] and Calculated Isotropic Hyperfine Coupling Constants of $\dot{P}F_5^-$ [b]

	exptl[a]	calcd
a_P^{iso}	1356	1323
$a_{F^a}^{iso}$	3	−17
$a_{F^e}^{iso}$	197	174

[a] See ref 9. [b] Values in gauss.

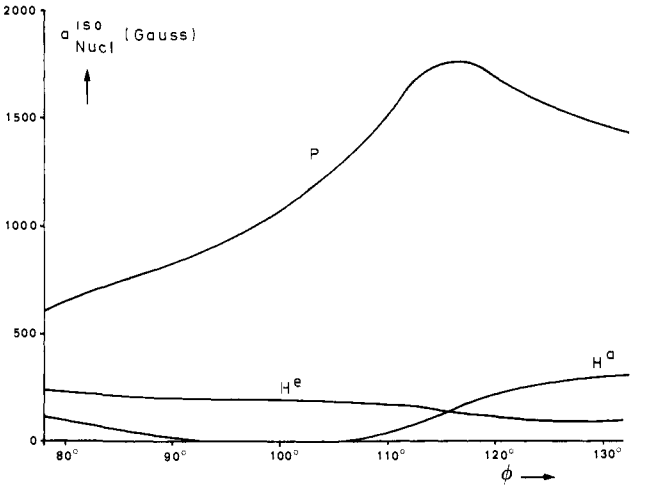

Figure 5. Calculated isotropic hyperfine coupling constants (a_{Nucl}^{iso}) of $H\dot{P}H_3$ as a function of the apical–equatorial bond angle ϕ; values for a_{Nucl}^{iso} are in gauss.

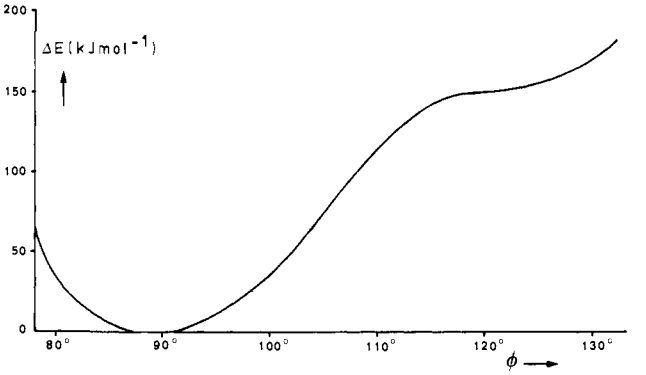

Figure 6. Energy of $H\dot{P}H_3$ as a function of the apical–equatorial bond angle ϕ relative to the optimized radical, values in kJ mol^{-1}.

(22) Coulson, C. A. *Nature (London)* **1969**, *221*, 1106.
(23) Bochvar, D. A.; Gambaryan, N. P.; Epshtein, L. M. *Russ. Chem. Rev. (Engl. Transl.)* **1976**, *45*, 660.
(24) Ratner, M. A.; Sabin, J. R. *J. Am. Chem. Soc.* **1977**, *99*, 3954.
(25) Halgren, T. A.; Brown, L. D.; Kleier, D. A.; Libscomb, W. N. *J. Am. Chem. Soc.* **1977**, *99*, 6793.
(26) Rauk, A.; Allen, L. C.; Mislow, K. *J. Am. Chem. Soc.* **1972**, *94*, 3035.
(27) Strich, A.; Veillard, A. *J. Am. Chem. Soc.* **1973**, *95*, 5574.
(28) Howell, J. M.; Van Wazer, J. R.; Rossi, A. R. *Inorg. Chem.* **1974**, *13*, 1747.
(29) Keil, F.; Kutzelnigg, W. *J. Am. Chem. Soc.* **1975**, *97*, 3623.
(30) Collins, J. B.; Schleyer, P. v. R.; Binkely, J. S.; Pople, J. A. *J. Chem. Phys.* **1976**, *64*, 5142.

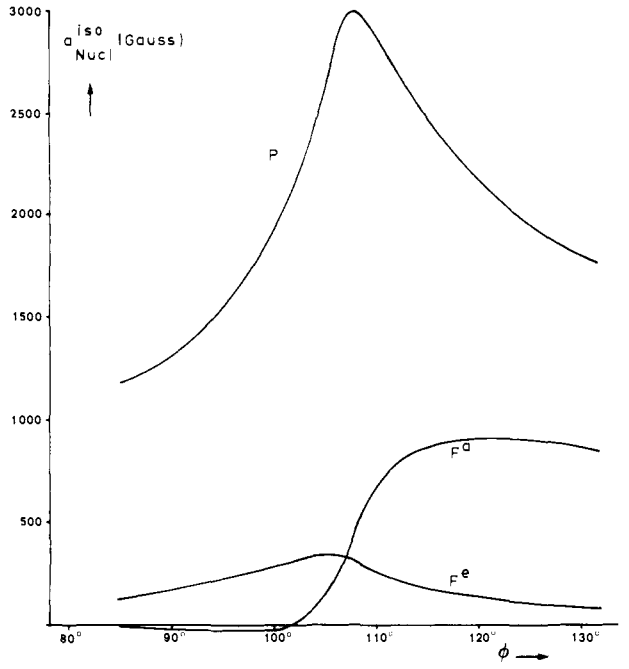

Figure 7. Calculated isotropic hyperfine coupling constants (a_{Nucl}^{iso}) of $\dot{P}F_5^-$ as a function of the apical–equatorial bond angle ϕ; values for a_{Nucl}^{iso} are in gauss.

tibonding orbital and is located between phosphorus and the apical ligand. This structure has been assigned to the $Ph_3\dot{P}Cl$ radical in order to explain the high spin density on the apical chlorine.[3] For a further insight in these differences, we have calculated the effect of geometry variations on the spin density distribution. For the $H\dot{P}H_3$ radical the angle ϕ between the apical and the three equatorial bonds was varied from 80° to 130°. During the variation of ϕ all bond lengths were fixed at the optimized values. The calculated isotropic hyperfine coupling constants arising from the Fermi contact integrals at the phosphorus and hydrogen nuclei are given as a function of ϕ in Figure 5. Figure 6 represents the corresponding UHF energy during this variation of ϕ relative to the energy of the optimized radical (−342.472 475 au). The phosphorus isotropic hyperfine coupling constant reaches a maximum value at ϕ = 117°. At this point the phosphorus $3p_z$ orbital inverts and gives no contribution to the spin density distribution. This is the transition point where the structure changes formally from TBP-a to σ^*–C_{3v}. Figure 6 indicates that the σ^*–C_{3v} arrangement lies some 150 kJ mol^{-1} above the optimized C_{3v} structure. Attempts to optimize the σ^* structure were not successful, but led to the dissociation into PH_3 and H· (vide infra). The most important difference between the TBP-a and the σ^*–C_{3v} radical is the distribution of the unpaired electron over the hydrogen atoms. The σ^*–C_{3v} arrangement is characterized by a high spin density in the C_3 axis of the radical. This results in large isotropic couplings on phosphorus and the apical hydrogen atom. Going from TBP-a toward σ^*–C_{3v} a continuous transfer of spin density from the equatorial nuclei to the apical nucleus has been calculated. This transfer starts at approximately ϕ = 108°, before the actual inversion takes place. Therefore a nonzero spin density on an apical ligand in a C_{3v} phosphoranyl radical gives no definite proof of a σ^*-arrangement. Nevertheless the calculated spin density distribution for the $H\dot{P}H_3$ σ^* structure is comparable with the experimental values of the $Ph_3\dot{P}Cl$ radical and supports the σ^* assignment for $Ph_3\dot{P}Cl$. For $\dot{P}F_5^-$ we have performed a similar structure variation of the bond angle ϕ. Variation of ϕ revealed a transition from O_h to σ^*–C_{4v} at ϕ = 108°. The calculated parameters (a_{Nucl}^{iso}, spin density in the valence p orbitals and UHF energy) are depicted in Figures 7–9. The energy difference between the optimized $\dot{P}F_5^-$ radical and its σ^*–C_{4v} arrangement is approximately 215 kJ mol^{-1}. Analogous to the C_{3v} radicals, there is a difference in the electronic structure of the optimized $\dot{P}F_5^-$ radical and its σ^*-arrangement. For the optimized octahedral

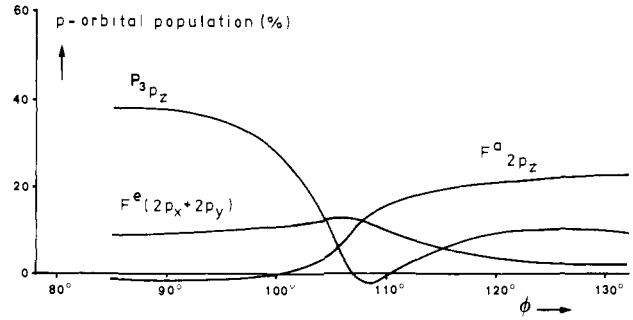

Figure 8. Calculated valence p orbital populations as a function of the apical–equatorial bond angle ϕ. Values are obtained from a Mulliken population analysis.

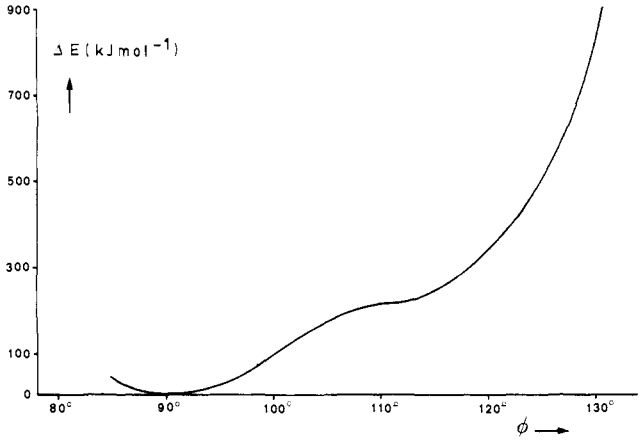

Figure 9. Energy of $\dot{P}F_5^-$ as a function of the apical–equatorial bond angle ϕ relative to the optimized radical, values in kJ mol^{-1}.

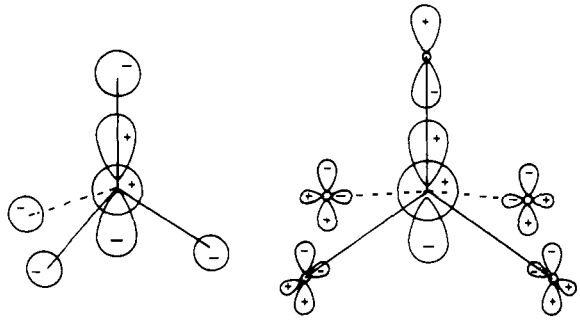

Figure 10. Schematic representation of the SOMOs of σ^*-arrangements of $H\dot{P}H_3$ and $\dot{P}F_5^-$.

structure the equatorial ligands possess a large spin density whereas the σ^*–C_{4v} radical is characterized by a high spin density on the apical ligand. Both the O_h and σ^* structure exhibit a large phosphorus isotropic hyperfine coupling. This relative high spin density in the C_4 axis of the $\dot{P}F_5^-$ radical anion possessing a σ^*-arrangement is comparable with the experimental values of the related C_{4v} $Cl\dot{P}(O_2C_6H_4)_2^-$ radical where a high spin density in the P–Cl axis has been found. From this point of view it may be suggested that the $Cl\dot{P}(O_2C_6H_4)_2^-$ radical anion possesses a σ^*–C_{4v} structure. This possibility was already recently suggested by Symons.[31] Figure 10 gives a schematical representation of the SOMO for the σ^* structures of $H\dot{P}H_3$ and $\dot{P}F_5^-$.

IV. Stability of $X^a\dot{P}H_3$ radicals

As we showed in section III(1) the optimized C_{3v} $H\dot{P}H_3$ radical possesses a TBP-a structure. The question arises of whether this optimized structure represents the only stable structure for the

(31) Symons, M. C. R. "Electron Spin Resonance"; Ayscough, P. B., Ed.; The Chemical Society; London, 1982; Specialist Periodical Report, Vol. 7.

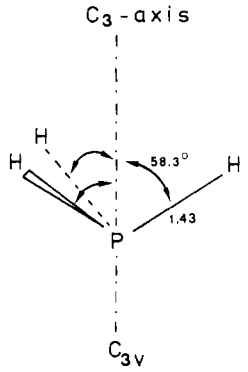

Figure 11. C_{3v} optimized geometry for PH_3 (E(UHF) = −342.025 690 au).

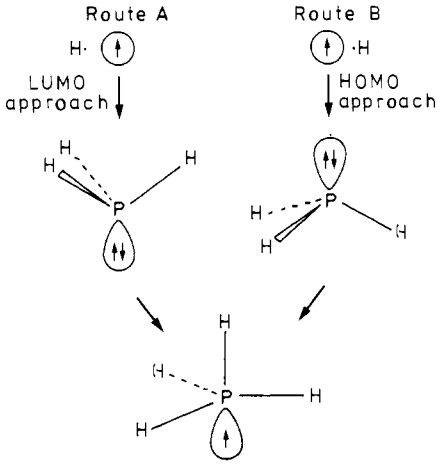

Figure 12. Two possible routes for H· attack toward PH_3. Route A, LUMO approach; route B, HOMO approach.

C_{3v} $H\dot{P}H_3$ radical. In principle it could be possible that there are more stable geometries for a C_{3v} $H\dot{P}H_3$ radical. Furthermore it is important to know the stability of the C_{3v} $H\dot{P}H_3$ radical, for example, with respect to the dissociation into PH_3 and H·.

(1) Potential Surface PH_3 + H·. The PH_3 molecule is pyramidal and possesses a C_{3v} geometry. In its 4-31G optimized structure the P–H bond length is 1.43 Å, and the angle between each P–H bond and the C_3 axis is 58.3° (Figure 11).

The calculated energy difference between the optimized C_{3v} $H\dot{P}H_3$ radical and the sum of isolated PH_3 and H· is 0.051 449 au (135 kJ mol^{-1}) in favor of the dissociation. The HOMO of PH_3 contains the two nonbonding electrons. Attack of a hydrogen atom along the PH_3 C_3 axis leads to a C_{3v} $H\dot{P}H_3$ radical. There are two possible routes for this attack (Figure 12): an approach of H· toward the LUMO of the PH_3 molecule or an approach toward the HOMO. Likewise the dissociation of a C_{3v} $H\dot{P}H_3$ radical can proceed along these two routes. To determine the route with the lowest energy barrier three cross sections through the multidimensional potential energy surface were calculated. For each cross section the equatorial bond lengths (r_e) were kept constant while the apical bond length (r_a) and the apical–equatorial bond angle (ϕ) were varied from 1.4 to 4.3 Å and from 55° to 125°, respectively. Cross sections were calculated for r_e = 1.4, 1.5, and 1.6 Å (Figure 13). The potential surfaces differ in the number of minima and transition states. For the r_e = 1.6 Å surface three minima were calculated, one for a stable TBP-a radical (r_a = 1.43; ϕ = 89.5°) and two "loose complexes", for both HOMO approach (r_a = 3.90; ϕ = 123.4°) and LUMO approach (r_a = 4.29; ϕ = 56.6°). On this surface there are two transition states (TS). The HOMO-TS possesses a perfect tetrahedral geometry (r_a = 1.60; ϕ = 109.4°) and a symmetrical SOMO (i.e., only the s orbitals of phosporus and hydrogen are involved). The phosphorus Fermi contact integral is, due to the absence of $3p_z$ contribution, very high (2.265 electrons Bohr^{-3}; a_P^{iso} = 1698 G), and a considerable amount of spin density is found on the four equivalent hydrogen nuclei (0.099 electrons Bohr^{-3}; a_H^{iso} = 158 G). The LUMO-TS (r_a = 1.82; ϕ = 73.9°) lies 41.1 kJ mol^{-1} below the HOMO-TS. The electronic structure of this LUMO-TS is characterized by a low phosphorus Fermi contact integral (0.368 electrons Bohr^{-3}; a_P^{iso} = 238 G) and a high value on the approaching hydrogen nucleus (0.216 electrons Bohr^{-3}; a_H^{iso} = 345 G). SOMOs of both transition states are depicted in Figure 14.

Table V. Energies[a] of the Minima and Transition States on the Cross Sections of the Potential Surface

	r_e = 1.6 Å	r_e = 1.5 Å	r_e = 1.4 Å
C_{3v} radical	0.051 494 (135.2)	0.055 675 (146.2)	
LUMO-TS[b]	0.079 576 (208.9)	0.069 342 (182.1)	
HOMO-TS[b]	0.095 208 (250.0)		
LUMO-LC[c]	0.022 120 (58.1)	0.004 045 (10.6)	0.001 106 (2.9)
HOMO-LC[c]	0.022 094 (58.0)	0.004 016 (10.5)	0.001 062 (2.8)

[a] Energies are relative to PH_3 + H· (−342.523 923 au). Values between brackets refer to differences in kJ mol^{-1}. [b] TS = transition state. [c] LC = loose complex.

For the r_e = 1.5 Å surface again three minima were calculated. The TBP-a radical (r_a = 1.44 Å; ϕ = 89.0°), the HOMO-loose complex (r_a = 3.89 Å; ϕ = 122.5°), and the LUMO-loose complex (r_a = 4.23 Å; ϕ = 57.5°). On this surface only one transition state, namely for the LUMO approach, is found (r_a = 1.76 Å; ϕ = 78.6°). Its structure is comparable with the LUMO-TS on the r_e = 1.6 Å surface. Finally the r_e = 1.4 Å surface possesses only two specific points; a HOMO-loose complex (r_a = 3.86 Å; ϕ = 121.2°) and a LUMO-loose complex (r_a = 4.17 Å; ϕ = 58.8°). Table V summarizes the energies of the various minima and transition state relative to the energy of isolated PH_3 and H· (−342.523 923 au). *From these potential surfaces it is clear that the TBP-a structure represents the only stable $H\dot{P}H_3$ radical.* None of the surface indicates a minimum that could belong to a stable σ^*–C_{3v} arrangement. *The potential surface shows furthermore that the energy barrier for LUMO approach is smaller than for HOMO approach.* We have calculated fully optimized structures for the HOMO- and LUMO-loose complexes. Their PH_3 fragments are identical with each other and with the optimized PH_3 molecule. The P–H[a] distances differ: 4.18 Å for the LUMO and 3.86 Å for the HOMO. The energy of these loose complexes lies slightly below that of the isolated PH_3 + H·. This difference has no physical significance and is probably due to a small calculated interaction between the outer 4-31G orbitals of PH_3 and H·. Using the saddle-point optimization method, we have optimized the LUMO-TS with respect to all geometric parameters within C_{3v} symmetry (Figure 15). This LUMO-TS lies 178.3 kJ mol^{-1} above the isolated PH_3 + H· and 43.2 kJ mol^{-1} above the optimized C_{3v} $H\dot{P}H_3$ radical. This demonstrates that the dissociation of $H\dot{P}H_3$ is not a wholly downhill process as previously suggested by Howell et al.[7] Despite many trial geometries we were not able to calculate a saddle point that could be attributed to a HOMO-TS. All efforts led to nonoptimized structures with very short apical bonds and large values of ϕ or to the previously optimized LUMO-TS. For the C_{3v} $H\dot{P}H_3$ radical, the LUMO-TS, and both loose complexes we have calculated correlation energies by Møller–Plesset perturbation theory (UMP2 and UMP3) and configuration interaction. These values are listed in Table VI. The post SCF calculations do not change the conclusions based on the UHF calculations. The energy difference between LUMO-TS and isolated PH_3 + H· is lowered from 178.3 to 147.9 kJ mol^{-1} after configuration interaction, while the stability of the C_{3v} radical relative to the LUMO-TS rises from 43.2 to 51.1 kJ mol^{-1} (Table VI). *The most important result that can be derived from the potential surfaces is that for all geometries where the electronic structure is σ^*–C_{3v} the radical dissociates directly without any energy barrier* (Figure 13). Therefore the ligand exchange processes of nonrigid TBP-e phosphoranyl radicals via

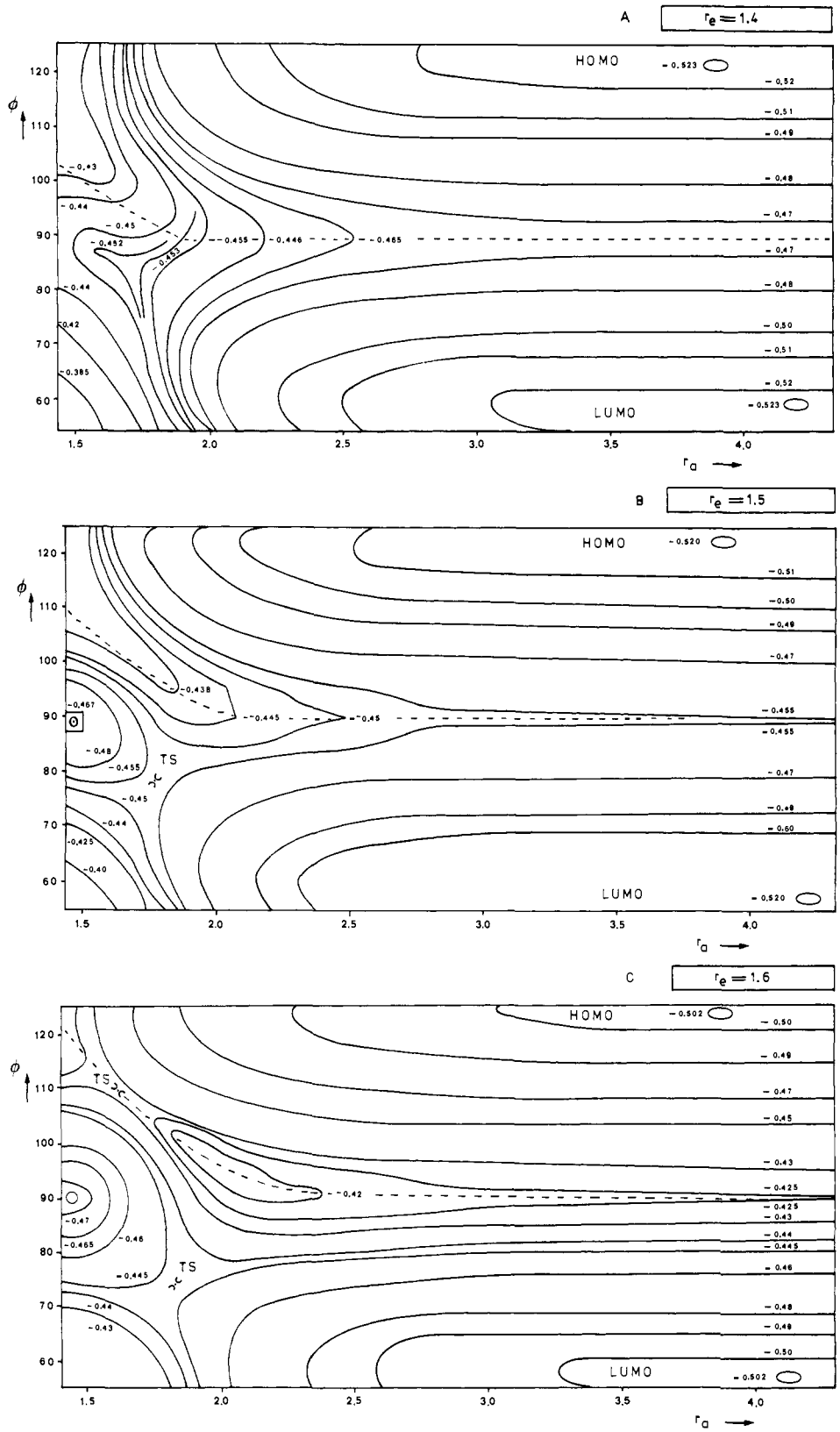

Figure 13. Potential energy surfaces of the $PH_3 + H\cdot$ system. Geometric parameters are r_a, r_e, and ϕ (see text). Cross sections are drawn for three values of r_e: (A) r_e = 1.4 Å, (B) r_e = 1.5 Å, (C) r_e = 1.6 Å. The dotted lines indicate the edge between TBP-a and σ^* structures.

a σ^* intermediate[32] seem questionable.

(2) Stability of $F\dot{P}H_3$ and $Cl\dot{P}H_3$. The energy of $F\dot{P}H_3$ lies 120.9 kJ mol^{-1} above the energy of isolated PH_3 and F·. The geometry of this radical differs from the related radicals (Table I). The equatorial bond length of 1.43 Å is considerably shorter than that of the same bond in $H\dot{P}H_3$ (1.59 Å) but identical with the bond length in the PH_3 molecule. The angle ϕ (85.9°) is smaller and the P–F bond length of 1.79 Å is longer than for $F\dot{P}F_3$ and $F\dot{P}Cl_3$. This structure actually resembles the LUMO-TS for $H\dot{P}H_3$. As in the case of $H\dot{P}H_3$, we have found two loose complexes for $F\dot{P}H_3$ both for HOMO and LUMO approach. Their PH_3 fragments are identical with the PH_3 molecule, the P–F distances are 3.21 and 3.73 Å, respectively. By means of the

(32) Roberts, B. P., Singh, K. *J. Chem. Soc., Chem. Commun.* **1979**, 980.

Table VI. Correlation Energies[a] of $H\dot{P}H_3$ for the Optimized Structures and the Transition State

	E(UHF)	E(UMP2)	E(UMP3)	E(CID)
C_{3v} radical	−342.472 475 (135.1)	−342.555 382 (114.8)	−342.572 836 (105.9)	−342.582 713 (96.8)
LUMO-TS	−342.456 009 (178.3)	−342.537 795 (160.9)	−342.554 448 (154.2)	−342.563 243 (147.9)
LUMO-LC	−342.523 978 (−0.2)	−342.599 037 (0.0)	−342.613 133 (0.0)	−342.619 516 (0.0)
HOMO-LC	−342.524 016 (−0.2)	−342.599 090 (−0.1)	−342.613 186 (−0.1)	−342.619 570 (−0.2)
PH_3 + H·	−342.523 923	−342.599 056	−342.613 152	−342.619 497

[a] Values between brackets refer to differences relative to PH_3 + H· in kJ mol^{-1}.

Table VII. Energies[a] and $\langle S^2 \rangle$ Values of the Optimized Structures and the Transition State of $F\dot{P}H_3$ and $Cl\dot{P}H_3$

	$F\dot{P}H_3$		$Cl\dot{P}H_3$	
	E(UHF)	$\langle S^2 \rangle$	E(UHF)	$\langle S^2 \rangle$
TBP-a	−441.245 124 (120.9)	0.7579		
LUMO-TS	−441.241 399 (130.7)	0.7819		
LUMO-LC	−441.291 240 (−0.2)	0.7508	−800.997 249 (−0.2)	0.7502
HOMO-LC	−441.292 633 (−3.8)	0.7509	−801.000 448 (−8.6)	0.7510
PH_3 + X^{a}·	−441.291 171	0 + 0.7500	−800.997 165	0 + 0.7500

[a] Values between brackets refer to differences relative to PH_3 + X^{a}· in kJ mol^{-1}.

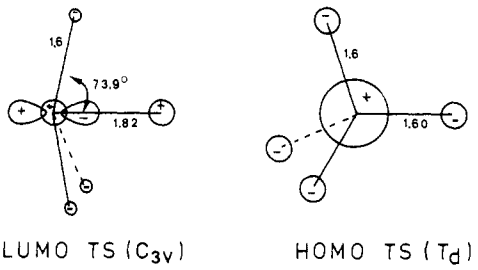

Figure 14. SOMOs for the transition states for LUMO and HOMO approach on the r_e = 1.6 Å surface.

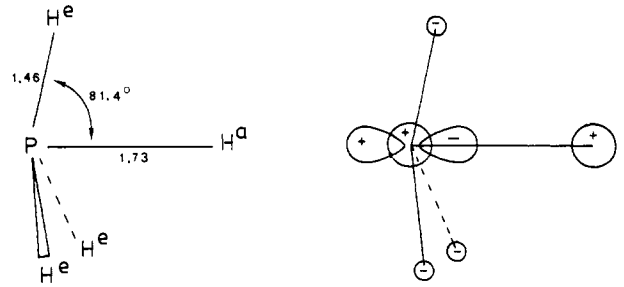

Figure 15. LUMO-TS of the PH_3 + H· ⇄ $H\dot{P}H_3$ system. Calculated isotropic hyperfine coupling constants are a_P^{iso} = 199, $a_{H^a}^{iso}$ = 260, and $a_{H^e}^{iso}$ = 124 G.

saddle-point optimization method the F-PH_3 transition state for LUMO approach was calculated. Its structure (Figure 16) and energy (Table VII) are close to those of the optimized $F\dot{P}H_3$ radical.

The energy of this transition state is 130.7 kJ mol^{-1} higher than the isolated PH_3 and F·. The energy difference between $F\dot{P}H_3$ radical and transition state is only 9.8 kJ mol^{-1} indicating that the radical is rather unstable. In section III(1) of this paper we mentioned that for $Cl\dot{P}H_3$ no stable geometry could be calculated. On attempted optimization all trial geometries revealed a HOMO-loose complex (PH_3 + Cl·; distance 3.21 Å) or a LUMO-loose complex (PH_3 + Cl·; distance 4.18 Å). The energies of these loose complexes are essentially the same as for the isolated PH_3 and Cl· (Table VII).

V. Conclusions

The calculations showed that all studied C_{3v} $X^{a}\dot{P}X^{e}_3$ phosphoranyl radicals possess a TBP-a structure. The calculated electronic structure of these radicals is in good agreement with the experiments on the $\cdot\overline{P(OCH_2CH_2)_3N}^{+}BF_4^{-}$ radical. Geometry variations for $H\dot{P}H_3$ reveal a σ^*-arrangement, which, however, is unstable and dissociates directly into PH_3 and H·. The calculated electronic structure of this σ^*-arrangement is comparable with the experimental values for the $Ph_3\dot{P}Cl$ radical reported by Berclaz et al.[3] and therefore gives support to their σ^*-assignment. The structure of C_{4v} $\dot{P}F_5^-$ is octahedral with the unpaired electron in apical position. This structure is fully analogous to the TBP-a structures. The calculated isotropic hyperfine coupling constants of $\dot{P}F_5^-$ are in excellent agreement with the experimental values reported by Morton et al.[9] Variation of the apical–equatorial bond angle for $\dot{P}F_5^-$ leads to a σ^*-arrangement. Comparison of the electronic structures of this σ^* $\dot{P}F_5^-$ radical anion and the experimental values obtained for the $Cl\dot{P}(O_2C_6H_4)_2^-$ radical anion indicates that the latter possibly possess a σ^*-C_{4v} arrangement. Despite many geometry variations and a number of different radicals it was not possible to optimize the geometry of a σ^*-C_{3v} or σ^*-C_{4v} radical. This suggests that σ^* structures are not stable. Nevertheless the calculated electronic structures for the σ^*-arrangements of $H\dot{P}H_3$ and $\dot{P}F_5^-$ are in correspondence with the experimental values obtained for the $Ph_3\dot{P}Cl$ and $Cl\dot{P}(O_2C_6H_4)_2^-$, radicals, respectively. *It is possible that the apparent formation and existence of a σ^* structure for $Ph_3\dot{P}Cl$ and $Cl\dot{P}(O_2C_6H_4)_2^-$ is the result of the geometry of their precursors and of matrix effects which may prevent geometrical isomerizations and control cage reactions.* However, the possibility that $Ph_3\dot{P}Cl$ and $Cl\dot{P}(O_2C_6H_4)_2^-$ represent stable σ^* radicals cannot be excluded. The stability of these radicals should then be the result of a subtle intrinsic stabilizing energy effect which could not be abstracted from the calculations on the $H\dot{P}H_3$ and $\dot{P}F_5^-$ model systems. Therefore it may be of interest to mention the recent work of Clark[33] on the structure of H_3PX^{+}· radical cations (X = PH_3, H_2S, HCl), which revealed a σ^* structure for $H_3PPH_3^{+}$·. The $H_3PSH_2^{+}$· and H_3PClH^{+}· radical cations possess structures that deviate more or less from the ideal σ^* structure toward TBP-e. Clark pointed out that the existence of a σ^* structure is extremely dependent on the energy levels of the HOMO and SOMO of X and PH_3^{+}·

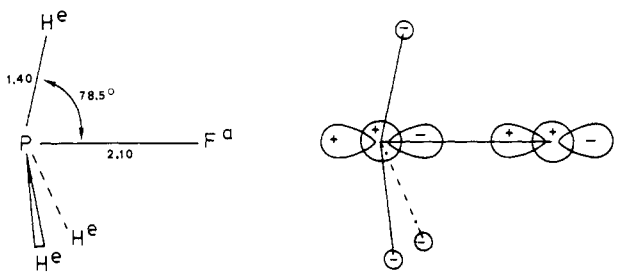

Figure 16. LUMO-TS of the PH_3 + F· ⇄ $F\dot{P}H_3$ system. Calculated isotropic hyperfine coupling constants of this structure are a_p^{iso} = 144, a_F^{iso} = 341, and a_H^{iso} = 48 G.

(33) Clark, T. *J. Comput. Chem.* **1983**,*4*, 404.

respectively. Only in the case that these energy levels are degenerated (or nearly) a σ^* structure can be expected.

Acknowledgment. This investigation has been supported by the Netherlands Foundation for Chemical Research (SON) with financial aid from the Netherlands Organization for the Advancement of Pure Research (ZWO).

Registry No. $H\dot{P}H_3$, 25530-87-4; $F\dot{P}F_2$, 14855-36-8; $F\dot{P}H_3$, 56360-19-1; $H\dot{P}F_3$, 56360-18-0; $\dot{P}F_5^-$, 89825-40-1; PH_3, 7803-51-2; H·, 12385-13-6; $Cl\dot{P}H_3$, 89746-27-0; $Cl\dot{P}F_2$, 89746-28-1; $H\dot{P}Cl_3$, 89746-29-2; $F\dot{P}Cl_3$, 89746-30-5; $Cl\dot{P}Cl_3$, 20762-59-8.

Electronic Structure of 1,5-Dithia-2,4,6,8-tetrazocine. Model Calculations and Spectroscopic Investigations

Rolf Gleiter,*† Richard Bartetzko,† and Dieter Cremer‡

Contribution from the Institut für Organische Chemie der Universität Heidelberg, D-6900 Heidelberg, West Germany, and the Lehrstuhl für Theoretische Chemie der Universität Köln, D-5000 Köln, West Germany. *Received September 30, 1983*

Abstract: Model calculations (ab initio and MNDO) on 1,5-dithia-2,4,6,8-tetrazocine (**2**) show that the electron-rich 10-π system prefers a planar monocyclic structure. π-Donor substituents can, however, induce a pseudo-Jahn-Teller distortion leading to a bicyclic 8-π system with a transannular S–S bond. The results of these model calculations are substantiated by investigation of the newly synthesized 3,7-di-*tert*-butyl derivative of **2** (**5**), the 3,7-diphenyl derivative (**3**), and the 3,7-bis(dimethylamino) derivative (**4**) by means of He I PE spectroscopy and linear dichroic absorption spectroscopy in the visible and near-UV region. The results obtained are best understood by assuming $b_{1u}(\pi)$ and $a_u(\pi)$ as the two highest occupied and $b_{2g}(\pi)$ and $b_{3g}(\pi)$ as the lowest unoccupied MOs of **2**.

The structure of S_4N_4 (**1a**) can be deduced by starting with a planar ring (**1b**) in which each sulfur center contributes two electrons and each nitrogen one to the π system, leading to 12 π electrons.[1,2] The degeneracy of the half-filled highest occupied e_g orbital of **1b** (D_{2h}) is removed by forming two transannular S–S bonds in **1a** (D_{2d}). If one adopts this point of view the related system of 1,5-dithia-2,4,6,8-tetrazocine (**2**) in which two opposite sulfur centers of **1** are formally replaced by carbon centers should have 10 π electrons if planar since each carbon contributes one π electron to the π system.

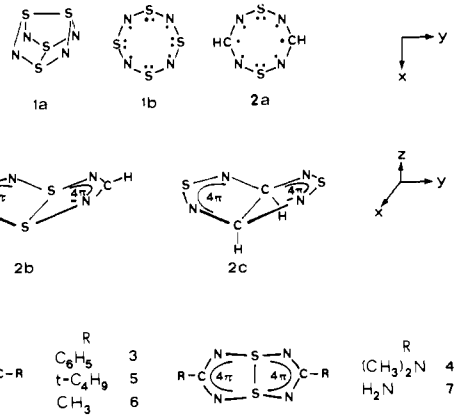

Recently derivatives of **2** have been synthesized,[3] and it has been shown by means of X-ray analysis that the 3,7-diphenyl derivative of **2** (**3**) has a planar eight-membered ring with an average S–N distance of 1.564 Å and an average C–N distance of 1.323 Å. The two phenyl groups are only slightly (9.7°) distorted out of the plane. It is interesting to note that the 3,7-bis(dimethylamino) derivative of **2** (**4**) shows a remarkable difference in its molecular shape. In contrast to the planar ring in **3**, the ring of **4** is folded along an axis through the two sulfur atoms with an interplanar angle of 101° thus giving rise to a transannular S–S distance of 2.428 Å, a value close to the transannular S–S distance found in S_4N_4 (2.58 Å). The average S–N distance (1.605 Å) as well as the average C–N distance in **4** (1.348 Å) is longer than the corresponding values found for **3**.[3]

Table I. Calculated Total Energies (hartree) and Energy Differences (kcal/mol) of **2a**, **2b**, and **2c**

basis	geometry[a]	2a	2b	2c
STO-3G	exptl	−1076.99720	−1077.06465	
		0	−42.3	
STO-3G	STO-3G	−1077.0273	−1077.06884	−1077.17102
		0	−26.0	−90.1
4-31G	exptl	−1088.08443	−1088.01958	
		0	40.7	
4-31G	STO-3G	−1088.09202	−1088.04741	−1088.02269
		0	28	43.5
STO-3G+d	exptl	−1077.53955	−1077.53750	
		0	1.3	
MNDO	MNDO	−58.24313	−58.21361	−58.16849
		0	18.5	25.3

[a] The experimental geometries **2a** and **2b** have been derived from reported data of **3** and **4**.

Both structural differences manifest themselves in the electronic absorption spectra. Compound **3** shows a long-wavelength band at 409 nm followed by a series of bands around 300 nm while **4** shows a maximum at 229 nm.

In order to understand the electronic structure of the eight-membered 1,5-dithia-2,4,6,8-tetrazocine ring, we have carried out model calculations on **2**. Furthermore, we have synthesized the 3,7-di-*tert*-butyl derivative of **2** (**5**). For **3**, **4**, and **5** we investigated the He (I) photoelectron (PE) spectra, and for **3** and **5** we recorded the electronic absorption spectra using the stretched film technique.[4]

† Universität Heidelberg.
‡ Universität Köln.

(1) Gleiter, R. *J. Chem. Soc.* **1970**, 3147.
(2) Gleiter, R. *Angew. Chem.* **1981**, *93*, 442; *Angew. Chem., Int. Ed. Engl.* **1981**, *20*, 444.
(3) Ernest, I.; Holick, W.; Rihs, G.; Schomburg, D.; Shohan, G.; Wenkert, D.; Woodward, R. B. *J. Am. Chem. Soc.* **1981**, *103*, 1540.

0002-7863/84/1506-3437$01.50/0